J Mater Sci (2010) 45:2564–2573
DOI 10.1007/s10853-010-4227-8

Microstructural evolutions in dissimilar welds between AISI 310 austenitic stainless steel and Inconel 657

H. Naffakh · M. Shamanian · F. Ashrafizadeh

Received: 28 September 2009 / Accepted: 11 January 2010 / Published online: 29 January 2010

Abstract This investigation has been performed to characterize dissimilar metal welds between type 310 austenitic stainless steel (SS) and Inconel 657 superalloy. The welds were produced using four types of filler materials: Inconel 82, Inconel A, Inconel 617, and type 310 SS. The weldments were characterized in detail using optical metallography and scanning electron microscopy. It can be concluded that Inconel A weld metal does not promote severe hot cracking. Continuous NbC precipitates in the Inconel 82 weld metal can sensitize the weld metal to solidification cracking. The presence of high amounts of Mo in Inconel 617 weld metal led to the formation of brittle phases. In addition, continuous precipitates were observed in the 310 SS weld metal, which can lead to poor resistance of the weld metal to hot cracking. In the aged condition, Inconel 82 and Inconel A exhibited good thermal stability, whereas Inconel 617 and type 310 SS exhibited poor thermal stability. Also, after subjecting the heat-affected zone and interface between Inconel weld metal and base metals to aging treatment, unmixed zone of Inconel 657 base metal side has disappeared. Elimination of this region can be attributed to high-temperature interdiffusion of alloying elements. Finally, it is found that Inconel A and Inconel 82 weld metals are the best choices for the dissimilar welds performed here, respectively.

H. Naffakh (✉) · M. Shamanian · F. Ashrafizadeh
Department of Materials Engineering, Isfahan University of Technology, Isfahan 84156-83111, Iran
e-mail: Homam-naffakh@ma.iut.ac.ir

H. Naffakh · F. Ashrafizadeh
Steel Institute, Isfahan University of Technology, Isfahan 84156-83111, Iran

Introduction

AISI type 310 austenitic stainless steel (SS) is one of the most important engineering materials used in high-temperature severe conditions. This material has extensive applications at elevated temperatures [1, 2]. In addition to austenitic SSs, the nickel and nickel–chromium-based superalloys have found suitable applications in oil and gas industries because of their high resistance to corrosion, hot oxidation, fatigue, and creep rupture. Chromium in these alloys forms the adherent oxide layer that can protect the alloy from detrimental oxygen attack. On the other hand, nickel improves high-temperature strength and resistance to carburizing atmospheres [3, 4].

ASTM A560 alloys, which have found many applications in high-temperature industries, consist of three grades of nickel–chromium-based superalloys. The type which contains 40–45 wt% Cr, 50–55 wt% Ni, and 1–2 wt% niobium has been introduced as Inconel 657 commercially. This alloy can tolerate high temperatures up to 1090 °C and resist detrimental conditions produced by fuel ash products, such as vanadium pentoxide and alkali metal sulfate compounds. Oil and gas refining industries have used this alloy for more than 50 years. Inconel 657 can be used to produce structural members, containers, supports, hangers, dampers, and spacers [5].

Type 310 SS can be joined using conventional fusion welding techniques, such as shielded-manual arc welding (SMAW), gas tungsten-arc welding (GTAW), and gas metal-arc welding (GMAW). Welding of 310 SS can be achieved with 310 SS filler material. In addition, for welding of Inconel 657, ENiCr-4 electrode or Inconel 617 filler wire and electrode is recommended, and all the SMAW, GTAW, and GMAW techniques can be employed for welding. Applying Inconel 657 alloy as heat-flow controlling

components (dampers) and supports (hangers) in reformer towers is highly recommended. The rotating axles, which control the damper motion, are made-up of 310 SS because they are exposed to lower temperatures. To join the dampers to the axles located in the wall tower, fusion welding is the normal process. Nevertheless, there are a few studies in the literature, investigating the proper filler material, microstructural features, physical and mechanical properties of the weld, and weldability of such dissimilar joints between 310 SS and Inconel 657. Therefore, the main purpose of this article is to investigate the effects of aging treatment (at 1000 °C for 100 h) on microstructure [fusion zone (FZ), heat-affected zone (HAZ), partially melted zone (PMZ), and unmixed zone (UZ)] and thermal stability of the joints (between 310 austenitic SS and Inconel 657 superalloy) that have been individually welded under constant welding parameters (i.e., constant heat inputs and dilutions) in order to identify the most appropriate filler material.

Experimental procedure

The nominal composition of the base metals is presented in Table 1. The type 310 SS had been hot-rolled, water-quenched, and finally solution-annealed to dissolve any precipitates. The Inconel 657 superalloy was obtained as a plate in the as-cast condition. Samples of both materials were then prepared with dimensions 160 × 60 × 12 mm (length × width × thickness). The Inconel 82, Inconel 617, Inconel A, and type 310 SS filler material were also supplied for this study. The nominal composition of the filler metals and electrodes differed primarily in their Cr, Ni, Nb, and cobalt content. Inconel 82, Inconel A, and Inconel 617 contain niobium, whereas 310 SS does not (Table 1).

Two test plates with a 75°V groove were welded together with a 2.5 mm root opening gap and a root face of 1 mm. Welding was performed using manual GTAW butt weld process with filler wires of 2.5-mm diameter to deposit to passes of Inconel 82 filler metal, or by manual SMAW with a coated electrode of 3.25 mm diameter to deposit Inconel A, Inconel 617, and 310 SS electrodes. The weld metal deposited by the GTAW process was shielded by argon gas. After each deposited pass, the weld temperature was allowed to decrease below 150 °C before performing the next pass. Before welding, the test plates were clamped; after each weld pass, the weld surfaces were cleaned with a SS brush. The welding voltage (E), current (I), and speed (V) were simultaneously recorded during welding. The welding parameters were adjusted to obtain proper fluidity of the molten pool for all the fillers and coated electrodes. The welding parameters are presented in Table 2. Weldments were sectioned in axis length perpendicular to the weld fusion line to obtain samples for microstructural analysis. The metallographically prepared specimens were etched using Marble's solution (10 g $CuSO_4$ + 50 mL HCl + 50 mL H_2O). Each weldment was examined using optical metallography and scanning electron microscopy (SEM). The SEM was equipped with an energy dispersive X-ray spectrometer (EDS) for microanalysis. In accordance with the design requirements for qualifying welding consumables for oil industry service, the weld metal specimens were also investigated after subjecting them to an embrittling heat treatment at 1000 °C for 100 h.

Results and discussion

Microstructural of the base metals

Figure 1a shows the microstructure of the type 310 austenitic SS. Since this steel was water-quenched after hot rolling, the final structure consists of fine equiaxed grains

Table 1 Chemical composition of the base metals and filler materials

Elements	Base metals		Filler materials			
	310 SS	Inconel 657	Inconel 82	Inconel 617	Inconel A	310 SS
C	Max 0.1	Max 0.2	Max 0.1	Max 0.1	Max 0.1	Max 0.1
Si	1	1	0.5	1	1	1
Mn	2	1	3	2	3	2
Fe	Rem.	1	3	5.5	12	Rem.
Cr	26	45	20	25	15	26
Mo	–	–	–	10	1.5	–
Co	–	–	–	10	–	–
Ti	–	–	1	0.6	–	–
Nb	–	1	3	1	2.5	–
Al	–	–	–	1	–	–
Ni	21	Rem.	Rem.	Rem.	Rem.	21
Cu	–	–	0.5	0.5	0.5	0.75

Table 2 Parameters of welding

Filler materials	Welding process	Pass number	Current (A)	Voltage (V)	Welding speed (mm/s)	Heat input (kJ/mm)	Total heat input (kJ/mm)
Inconel 82	GTAW	1	120	12	1	1.44	5.93
	GTAW	2	110	12	1.1	1.2	
	GTAW	3	110	14	0.85	1.81	
	GTAW	4	105	12	0.85	1.48	
Inconel A	GTAW	1	135	12	0.77	2.10	8.94
	SMAW	2	105	26	1.76	1.55	
	SMAW	3	105	24	1.43	1.76	
	SMAW	4	105	24	1.25	2.02	
	SMAW	5	105	24	1.67	1.51	
Inconel 617	GTAW	1	130	12	1.20	1.30	7.19
	SMAW	2	90	24	1.58	1.37	
	SMAW	3	110	24	1.15	2.30	
	SMAW	4	120	24	1.30	2.22	
310 SS	GTAW	1	130	12	1	1.56	6.49
	SMAW	2	100	25	3	.83	
	SMAW	3	110	25	1.88	1.33	
	SMAW	4	110	25	1.76	1.56	
	SMAW	5	110	22	2	1.21	

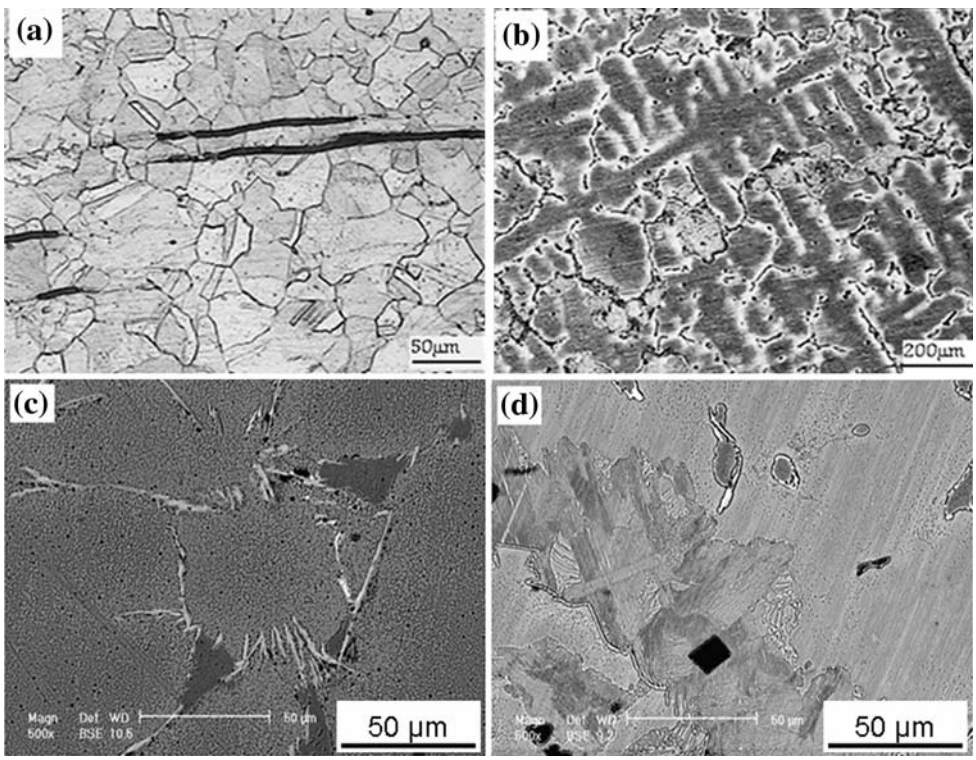

Fig. 1 The microstructure of **a** 310 austenitic SS, **b** Inconel 657 superalloy. **c** White γ/NbC structure and dark α-Cr phase. **d** Lamellar γ/Laves structure and cubic carbide precipitate

of austenite. No carbides or carbonitrides were observed in the microstructure, but delta ferrite stringers (elongated parallel to the rolling direction) were present in the austenite matrix.

Inconel 657 superalloy shows a relatively complex as-cast microstructure, which is completely dendritic and composed of columnar and equiaxed dendrites. This cast structure can be seen in Fig. 1b; interdentritic boundaries

have experienced severe segregation, which can be distinguished by their brighter color from darker dendritic cores. In this alloy, niobium has a strong tendency to partition to the liquid and form relatively low-melting terminal solidification products containing NbC and/or Laves phase. Several second phases can be observed in Fig. 1b, which is obtained in the interdentritic regions; white eutectic phases are the result of liquid transformation to austenite + niobium carbide (L → γ + NbC) in eutectic form. This structure is shown in the backscattered electron (BSE) image in Fig. 1c. This alloy contains 1–2 wt% niobium and small amounts of carbon. Therefore, the formation of this eutectic structure is expected. In previous investigations of nickel-base superalloys, this phase is termed "chinese script" [6]. These eutectic phases predominantly formed in the interdendritic regions. Furthermore, it can be seen that dark phases that are enriched in chromium, such as ferrite, are located near the γ-NbC structure (Fig. 1c). This phase has an important effect on toughness of the alloy at elevated temperatures. In addition, there is another type of eutectic structure in the alloy, which mainly forms at the grain boundaries and is fully lamellar. Figure 1d illustrates this structure, which is the result of liquid transformation to austenite + Laves (L → γ + Laves) eutectic structure at the last stages of solidification. It is clear that the γ/Laves structure has a lower melting point than γ/NbC structure and therefore has an important influence on the HAZ cracking of the alloy. Figure 1d shows the coarse cubic precipitates that appear dark in the BSE image, suggesting that they may contain light elements (such as C, N, or O). EDS revealed that coarse cubic precipitates were Cr-rich.

Microstructure weld metals

Inconel 82 weld metal

Figure 2a, b shows the FZ macro- and microstructure of the Inconel 82 weld metal, respectively. It can be seen that the microstructure is fully austenitic. The weld metal contains 3% Nb, which has the beneficial effect of increasing the thermal stability of the alloy for high-temperature operations. The Nb content in the Inconel 82 weld is enough to change the FZ solidification mode from cellular to dendritic. Hot cracking is caused and controlled by the presence and the amount of continuous phases in interdendritic regions. Nb is easily rejected into interdendritic regions (Fig. 2c) during solidification (equilibrium distribution coefficient of less than 1). In previous studies, differential thermal analysis indicated that Nb addition decreased the liquidus and solidus temperatures as well as increasing the solidification temperature range D_T ($D_T = T_L - T_S$, where T_L is liquidus temperature and T_S is solidus temperature) [6, 7]. This widening in solidification temperature range can increase sensitivity to solidification cracking. It is seen that continuous NbC precipitates (shiny) are formed in the interdendritic regions. Figure 2c reveals that niobium carbides are formed in the interdendritic regions and they are continuous. Based on this micrograph, Inconel 82 weld metal is susceptible to hot cracking [7]. TiC precipitates (darkly imaging) with a globular morphology are also formed in the intergranular regions, but this second phase is not continuous. This weld metal did not show the formation of other second phases (such as topologically closed phases).

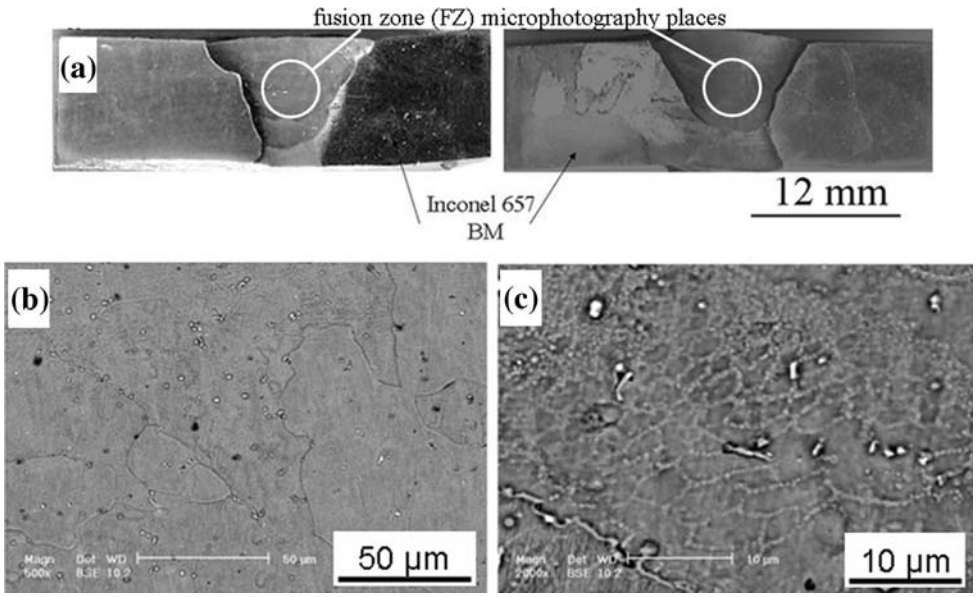

Fig. 2 **a** Macrophotograph of weld section displaying places of FZ microphotography. **b** Inconel 82 weld metal microstructure. **c** Inconel 82 weld metal microstructure in higher magnification. Precipitation of fine continuous NbC can be seen in the interdendritic regions

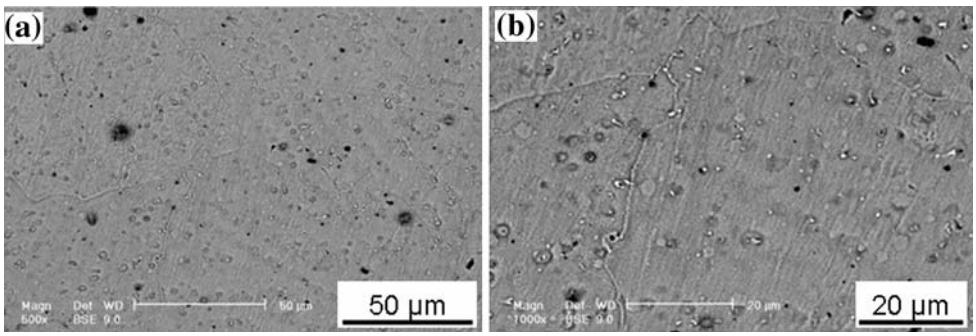

Fig. 3 **a** Inconel A weld metal microstructure. **b** Inconel A weld metal in higher magnification. Segregation of alloying element can be observed in the austenitic matrix

Inconel A weld metal

Figure 3 shows the FZ of the Inconel A weld metal. Although Inconel A weld metal, similar to Inconel 82, has considerable amounts of niobium (2.5%), its iron content (12%) is much greater than Inconel 82 weld metal (3 wt%). The presence of iron in nickel-based superalloys leads to a decrease in niobium solubility in the austenite phase. With the increased iron content in the nickel–chromium solid solution, the solubility of Nb is reduced. This can be observed in binary and ternary phase diagrams of these elements [6, 7].

Under these conditions, partitioning of Nb to the interdendritic regions in the weld metal is increased. Segregation of alloying elements leads to a broadening of the brittleness temperature range and constitutional supercooling can occur. It can change the mode of solidification from flat or cellular microstructure to columnar-dendritic microstructure [7–10]. But Fig. 3a, b does not show the formation of continuous network of NbC in the interdendritic or intergranular regions. The niobium carbides (brightly imaging particles in the BSE image) and oxide inclusions (black particles) are distributed in the austenite matrix. In contrast to the Inconel 82 weld metal, which a continuous network of niobium carbides is formed in its microstructure, there is no evidence of such continuous precipitates along the grain boundaries of Inconel A weld metal, although, NbC-distributed precipitates and oxide inclusion are formed. It can be attributed to the presence of higher amounts of nickel and less amount of chromium in Inconel A weld metal than that of Inconel 82 weld metal, which can dissolve the excessive amount of Nb. Such conditions are expected to decrease the hot cracking tendency of Inconel A weld metal [10]. Oxide inclusions in the weld metal reveal that the weld pool was not protected perfectly.

Inconel 617 weld metal

Figure 4 shows the FZ microstructure of Inconel 617 filler material. This displays the presence of a clear and distinctive columnar dendritic structure, in comparison to

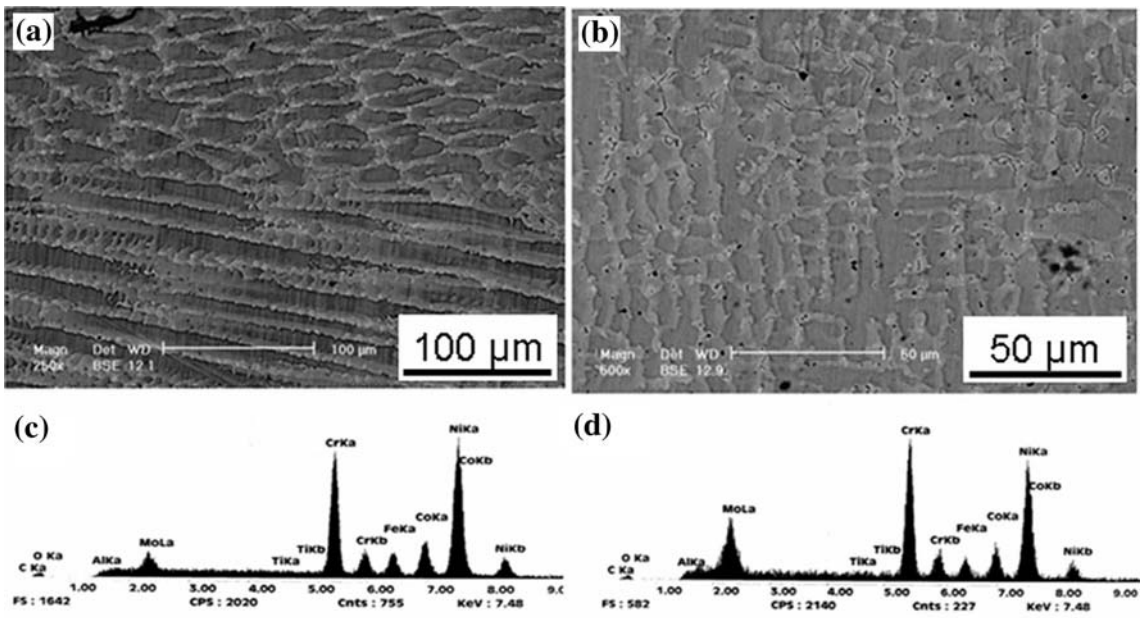

Fig. 4 **a** Inconel 617 weld metal microstructure. **b** Inconel 617 weld metal microstructure (perpendicular to dendrites). EDS for **c** dendritic core of Inconel 617 weld metal, **d** interdendritic region of Inconel 617 weld metal

Inconel 82 and Inconel A weld metal microstructures. In contrast to Inconel A and Inconel 82 weld metals, niobium content is low (1 wt%), but the amount of molybdenum (10 wt%) and cobalt (10 wt%) is high. Inconel 617 material has about 5.5 wt% iron that can limit solubility of Mo and Nb in austenite. The Mo partitioning coefficient decreases as the iron content in the weld increases (i.e., as the dilution level increases). These effects are controlled by the influence of Fe on the solubility of Mo and Nb in austenite and can be explained by the phase diagrams. These diagrams indicate that the maximum solid solubility of Mo in γ-Ni is 35 wt% (at 1200 °C), whereas a maximum of only 2.9 wt% Mo can be dissolved in γ-Fe (at ~1150 °C). A similar trend is observed for Nb, where the maximum solid solubility of Nb in γ-Ni is 18.2 wt% (at 1286 °C), whereas it is only 1.3 wt% at a similar temperature (1210 °C) in γ-Fe. Elements such as chromium and molybdenum have more tendencies to leave the dendritic cores and to be rejected to interdendritic regions [11–14]. Mo segregated from the solid to the liquid and the Mo-rich regions can be formed at the terminal stages of solidification (Fig. 4c, d). In the Inconel 617 weld metal, solidification initiates by L → γ (austenite) primary reaction, by which the γ dendrites reject Mo into the interdendritic liquid. As solidification progresses, the γ dendrites become richer in Mo at the solid/liquid interface until the maximum solid solubility of Mo in austenite is reached at the edge of the γ dendrites. According to Fig. 4, Tables 3 and 4, it can be said that since the interdendritic regions are enriched in Mo and the microstructure is consisted of fully coarse dendrites, thus the weld metal may have high tendency to embrittlement and solidification cracking [7, 10].

310 SS weld metal

The only austenitic SS filler material used in this study was 310 SS. Figure 5 illustrates the 310 SS FZ. The mode of solidification depends on welding parameters (heat input value, welding speed, inter-pass preheating) and chemical composition of the weld metal. As far as chemical composition is concerned, 310 SS filler material is simply composed of Fe, Cr, and Ni. These elements are well known for their low tendency to segregate in interdendritic and intergranular regions. Thus, it is expected not to be sufficient constitutional supercooling in order to alter the solidification mode from cellular to dendritic (Fig. 5a). Figure 5a shows that secondary arms have not developed and therefore the microstructure is cellular. Since the weld metal has some amount of copper, the formation of low-melting point phases, which make weld metal more prone to hot cracking, is probable. Figure 5b shows that low-melting point phases are located in the intergranular regions. According to this result, it can be expected that 310 SS weld metal exhibits poor resistance to hot cracking [7, 10].

Table 3 EDS data for dendritic core of Inconel 617 weld metal

Element	*K* ratio	Wt%	At.%
Al *K*	0.0017	0.173	0.364
Mo *K*	0.0554	5.544	3.287
Ti *K*	0.0016	0.160	0.189
Cr *K*	0.2382	23.820	26.085
Fe *K*	0.0641	6.415	6.534
Co *K*	0.1113	11.131	10.744
Ni *K*	0.5210	52.098	50.475
Total		100	100

Table 4 EDS data for interdendritic region of Inconel 617 weld metal

Element	*K* ratio	Wt%	At.%
Al *K*	0.0032	0.320	0.697
Mo *K*	0.1513	15.132	9.270
Ti *K*	0.0063	0.635	0.779
Cr *K*	0.2608	26.083	29.481
Fe *K*	0.0484	4.836	5.079
Co *K*	0.0924	9.239	9.214
Ni *K*	0.4313	43.130	43.176
Total		100	100

Aged weld metals

Figure 6a, b shows the microstructure of Inconel 82 weld metal after being in 1000 °C for 100 h. They reveal no considerable difference, when compare to unaged structure. But the formation of superior number of titanium carbide in grain boundaries in relation to unaged weld metal can lead to a decrease in the impact energy [15]. It can be seen that NbC precipitates in interdendritic regions are completely dissolved and some distributed NbC precipitates have remained. This microstructure indicates the thermal stability of Inconel 82 at elevated temperatures. Figure 7a, b exhibits the FZ of the Inconel A weld metal after aging. Experiencing high temperature for a relatively long time in this weld metal not only can eliminate severe segregation of interdendritic regions, but also can increase the size of initial precipitates. Microstructure of the aged weld metal proved that there is no new precipitation. Similar to Inconel 82 weld metal, Inconel A weld metal shows good thermal stability at elevated temperatures [15]. A continuous network of precipitates is formed along the grain boundaries and the microstructure is significantly

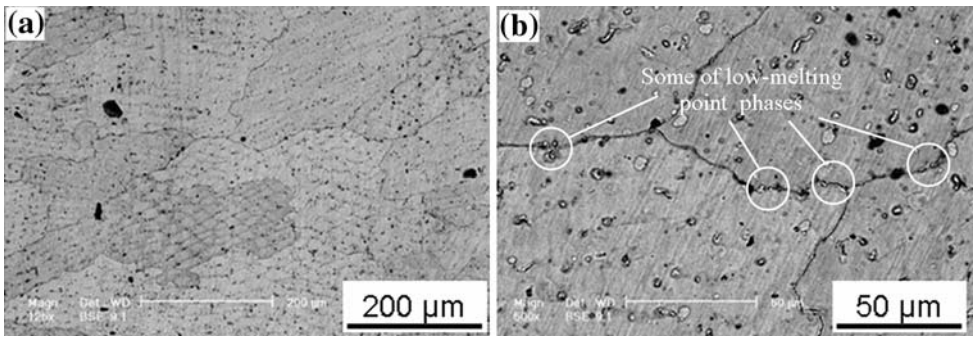

Fig. 5 **a** 310 SS weld metal microstructure. The weld metal is fully cellular. **b** 310 SS weld metal microstructure in higher magnification

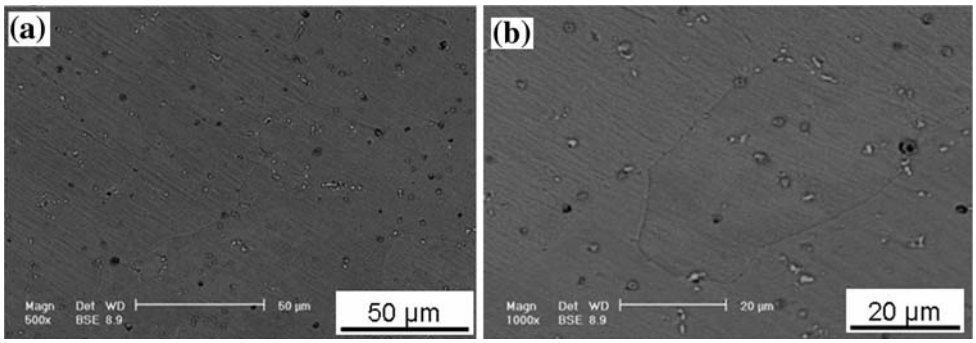

Fig. 6 Inconel 82 weld metal microstructure **a** after aging, **b** no continuous network of secondary phases

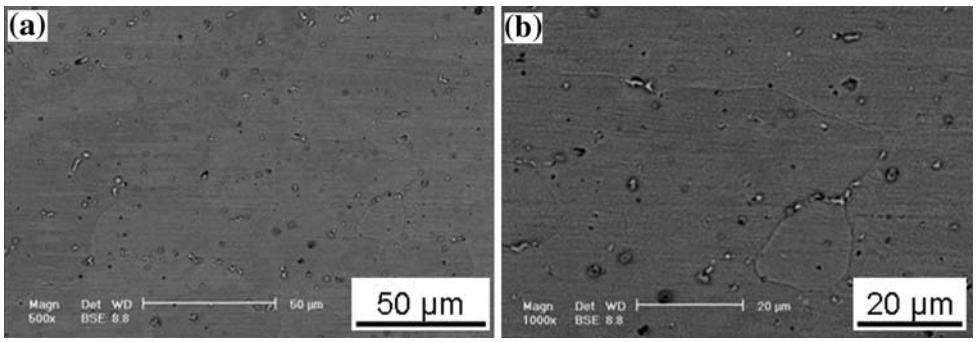

Fig. 7 Inconel A weld metal **a** after aging, **b** elimination of segregation

changed, by having the Inconel 617 weld metal subjected to the aging treatment (1000 °C for 100 h). Moreover, the aging leads to a formation of distributed precipitates within the grains (Fig. 8a, b). This precipitates-saturated microstructure can be more brittle than that of the aged Inconel 82 and Inconel A weld metals that do not have any continuous precipitates in the intergranular regions [15]. In the case of aged weld metal of 310 SS, formation of continuous chromium carbides, that can strongly influence the mechanical properties of the weldment, can be observed (Fig. 9). Based on the descriptions mentioned above and earlier published papers of the authors [7, 10, 15], the weldments produced by Inconel A and Inconel 82 exhibit the best mechanical properties (i.e., ultimate tensile strength, yield strength, elongation, and notch toughness), respectively.

Microstructure of UZ, PMZ, and HAZ before and after aging

For instance, the interface between Inconel 82 weld metal and Inconel 657 base metal is shown in Fig. 10a–c. The interface between Inconel 82 weld metal and 310 SS base metal is also presented in Fig. 10a, d, e. The UZ appears as a laminar layer, where a small fraction of the base metal has been totally melted and resolidified without undergoing any dilution. The microstructure of the HAZ for Inconel 657 side (Fig. 10b) shows extensive grain boundary melting and liquation. This PMZ is characterized by dendritic boundary melting and thickening. The tendency of dendrite boundaries in Inconel 657 to melt is attributed to their niobium enrichment; the presence of niobium at these boundaries not only lowers the melting point constitutionally, but also

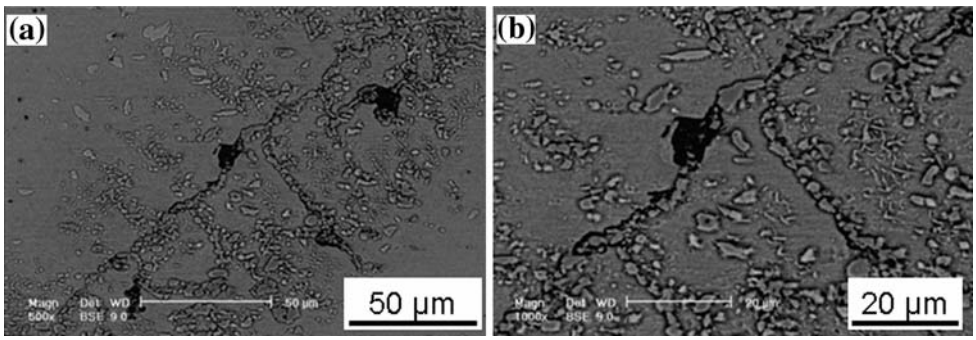

Fig. 8 Inconel 617 weld metal microstructure **a** after aging, **b** severe precipitation in the granular and intergranular regions

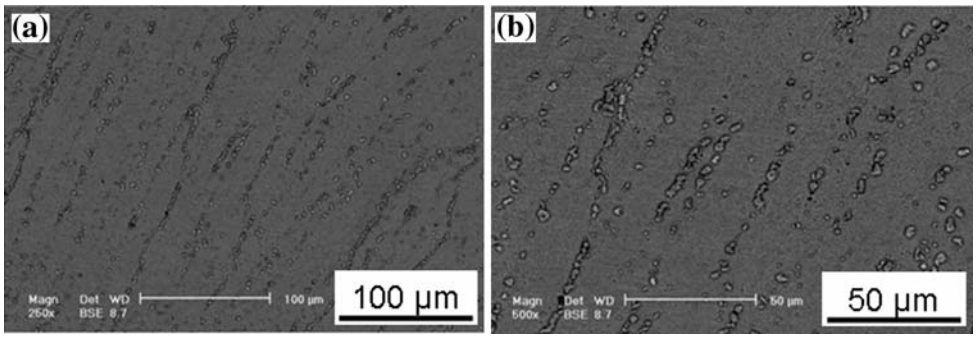

Fig. 9 310 SS weld metal **a** after aging, **b** in higher magnification

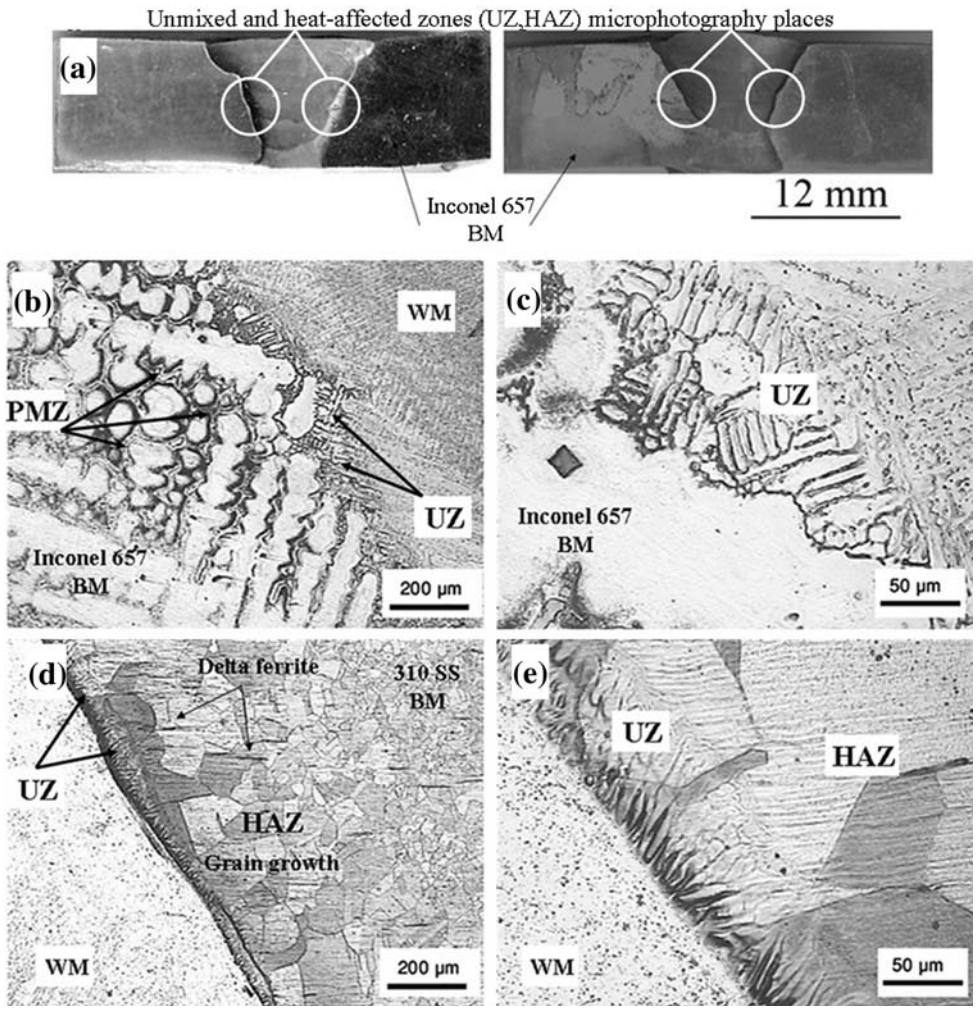

Fig. 10 **a** Macrophotograph of weld section displaying places of UZ and HAZ microphotography. **b** Microstructure of UZ, PMZ, and HAZ for Inconel 82 weldment before aging in Inconel 657 side. **c** Microstructure of BM and UZ in Inconel 657 side at higher magnification. **d** Microstructure of WM, BM, HAZ, and UZ in 310 SS side. **e** Microstructure of WM, HAZ, and UZ in 310 SS side at higher magnification

forms low-melting carbide-austenite eutectics during solidification. The PMZ in this side of the joint appears to be much wider, compared to the 310 alloy side (Fig. 10e).

On the other hand, remarkable grain growth occurred in 310 SS HAZ, which can be observed in Fig. 10d. The microstructure reveals the presence of ferrite stringers in some of the austenite grains within the base metal close to the HAZ. These ferrite stringers probably remained from the high-temperature primary processing of the base plate. Homogenization of such segregates cannot be effective, especially in austenitic alloys. The ferrite stringers have been expanded and grown in places close to the fusion boundary, presumably because more ferrite is usually retained during rapid cooling after the formation of delta ferrite due to the heating cycle.

After subjecting the HAZ and interface between Inconel weld metal and base metals to aging treatment, an interesting phenomenon has occurred: UZ of Inconel 657 base metal side has disappeared. Elimination of this region can be attributed to high-temperature interdiffusion of alloying elements. Diffusion at high temperature (1000 °C) for a relatively long time (100 h) can eliminate chemical composition variations between base metal and UZ. Therefore, a distinct boundary between these two regions, UZ and base metal, cannot be seen (Fig. 11a, b). Although severe segregation of interdendritic regions in Inconel 657 base metal has been removed, Nb-rich phases have remained relatively unchanged. Interdiffusion of alloying elements and elimination of boundary between UZ and 310 SS base metal can also be seen for interface of 310 SS base metal. Observations made on HAZ of 310 SS side exhibited that aging treatment does not cause any new precipitation and primary probable precipitates have been dissolved. Furthermore, region of grain growth after aging shows no considerable difference with HAZ of specimens in as-welded condition (Fig. 11c, d). Finally, it should be mentioned that transformation of delta ferrite to sigma ferrite due to aging treatment can significantly deteriorate impact toughness of 310 SS base metal [15].

Conclusions

Microstructure of Inconel 657 is composed of columnar and equiaxed dendrites. Several second phases were observed in the interdentritic regions. In the case of Inconel 82, it is seen that continuous NbC precipitates are formed in the interdendritic regions. Thus, Inconel 82 weld metal is sensitive to hot cracking. Inconel A weld metal does not show the formation of continuous NbC in the interdendritic or intergranular regions. Inconel 617 weld metal has a dendritic microstructure. This weld metal may have

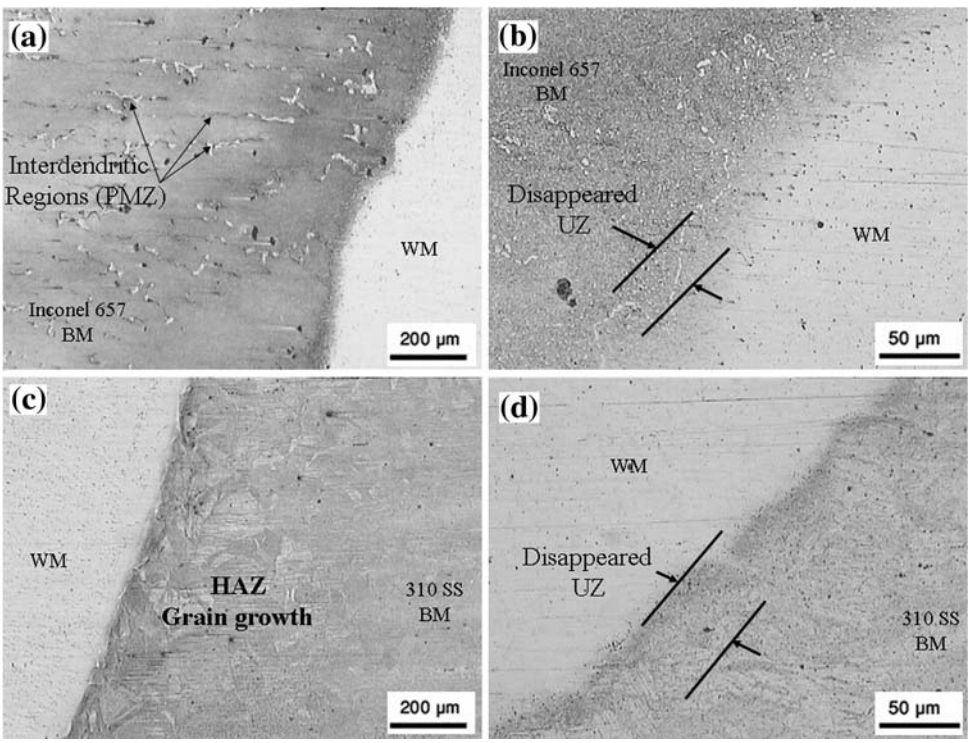

Fig. 11 Microstructure of disappeared UZ, PMZ, and HAZ in Inconel 82 weldment after aging: **a** WM, BM, PMZ, and disappeared UZ in Inconel 657 side; **b** BM, WM, and disappeared UZ in Inconel 657 side at higher magnification; **c** WM, BM, HAZ, and disappeared UZ in 310 SS side; **d** WM, HAZ, and disappeared UZ in 310 SS side at higher magnification

considerable tendency to embrittlement. In the case of 310 SS weld metal, formation of a continuous network of low-melting phases makes weld metal prone to hot cracking. After the aging heat treatment, the structures of Inconel 82 and Inconel A weld metal had no considerable difference with unaged structure. These microstructures well indicated the thermal stability at elevated temperatures. But Inconel 617 and 310 SS weld metals exhibited poor thermal stability. After subjecting the HAZ and interface between Inconel weld metal and base metals to aging treatment, UZ of Inconel 657 base metal side has disappeared. Elimination of this region can be attributed to high-temperature interdiffusion of alloying elements. Finally, it can be said that Inconel A and Inconel 82 weld metals are the best choices for the dissimilar welds performed here, respectively.

References

1. Kacar R, Baylan O (2004) Mater Des 25:317
2. Meola C, Squillace A, Memola F, Minutolo C, Morace RE (2004) J Mater Process Technol 155–156:1893
3. Jian L, Yuh CY, Farooque M (2002) Corros Sci 2:1573
4. Zhao SH, Xie X, Smith GD (2004) Surf Coat Technol 185:178
5. Belloni G, Caironi G, Gariboldi A, Lo Conte A (2001) SMiRT 16, Washington, DC (paper 1546)
6. Dupont JN, Banovic SW, Marder AR (2003) Weld J 82:125s
7. Naffakh H, Shamanian M, Ashrafizadeh F (2008) J Mater Sci 43:5300. doi:10.1007/s10853-008-2761-4
8. Kuo TY, Lee HT (2002) Mater Sci Eng A 338:202
9. Sireesha M, Albert SK, Shankar V, Sundaresan S (2000) Mater Sci Eng A 292:74
10. Naffakh H, Shamanian M, Ashrafizadeh F (2000) J Mater Process Technol 209:3628
11. Rowe MD, Crook P, Hoback GL (2003) Weld J 82:313s
12. Wang N, Mokadem S, Rappaz M, Kurz W (2004) Acta Mater 52:3173
13. Lee HT, Jeng SL, Yen CH, Kuo TY (2004) J Nucl Mater 335:59
14. Sireesha M, Albert SK, Shankar V, Sundaresan S (2000) J Nucl Mater 279:65
15. Naffakh H, Shamanian M, Ashrafizadeh F (2008) Metall Mater Trans A 39A:2403